Highly Viscous Phase Behavior of Organic-Rich Urban $PM_{2.5}$

Atta Ullah[1], Ji Yi Lee[2], Zhijun Wu[3], Kyoung-Soon Jang[4], Mijung Song[1,5]

[1]Department of Earth and Environmental Sciences, and Earth Environmental System Research Center, Jeonbuk National University, Jeollabuk-do Jeonju-si 54896, Republic of Korea; [2]Department of Environmental Science & Engineering, Ewha Womans University, Seoul 03760, Republic of Korea; [3]State Key Joint Laboratory of Environmental Simulation and Pollution Control, College of Environmental Sciences and Engineering, Peking University, Beijing 100871, China; [4]Bio-Chemical Analysis Team, Korea Basic Science Institute, Cheongju 28119, Republic of Korea; [5]Department of Environment and Energy, Jeonbuk National University, Jeollabuk-do Jeonju-si 54896, Republic of Korea

Correspondence to: Mijung Song (Mijung.Song@jbnu.ac.kr)

Summary: 11 pages, 2 figures, 2 table

S1. Chemical compositions of $PM_{2.5}$

The hourly mass concentration of $PM_{2.5}$ was measured by β-ray continuous ambient particle sensor (Thermo Scientific Inc., model 5014i, USA). The mass concentrations of inorganic ions, such as NO_3^-, SO_4^{2-}, NH_4^+, Cl^-, Na^+, Ca^{2+}, K^+, and Mg^{2+} were determined by ion chromatography (AQUION, Thermo Scientific, Massachusetts, USA) following procedures described in a previous study (Won et al., 2024). The mass concentrations of ammonium nitrate (AN) and ammonium sulfate (AS) were calculated from the measured nitrate and sulfate concentrations using Eqs. (S1.1) and (S1.2), respectively (Lan et al., 2018; Xue et al., 2023).

$$AN = NO_3^- \times 1.290 \quad \text{(S1.1)}$$

$$AS = SO_4^{2-} \times 1.375 \quad \text{(S1.2)}$$

The mass concentration of organic matter (OM) was determined by deducing the concentrations of inorganic compounds from the total $PM_{2.5}$. Meteorological parameters, including temperature and RH, were measured by the National Institute of Environmental Research in Seoul and an automated meteorological station (Met One Instruments, Inc., USA) in Beijing (Kim et al., 2022; Qiu et al., 2023). All meteorological data were averaged according to the filter sample intervals (from 10:00 to 09:00 local time the subsequent day). The O:C ratio of water-soluble organic compounds (WSOC) in the $PM_{2.5}$ filter-collected sample was measured by employing the Fourier-transform ion cyclotron resonance mass spectrometer (FT-ICR MS) as detailed in previous studies (Choi et al., 2017; Song et al., 2022).

S2. Extraction and droplet generation from $PM_{2.5}$ filters

The quartz filters containing $PM_{2.5}$ were cut into small pieces and extracted using a 1:1 (v/v) methanol-water solution, where methanol was high-performance liquid chromatography grade (Sigma-Aldrich), and water had a resistivity of 18.2 MΩ·cm (Millipore, USA). After extraction, the solution was sonicated for 1 hr at ~290 K and then filtered through a poly(ether sulfone) membrane with a 0.05 μm pore size. Micrometer-scale droplets were subsequently generated from the filtered extract using a nebulizer (MEINHARD, PerkinElmer, USA) and deposited onto a hydrophobic substrate (Hampton Research, Canada) (Song et al., 2025). This method primarily captures the water and methanol-soluble fraction of $PM_{2.5}$, as insoluble components are removed during filtration.

S3. Input parameters for COMSOL simulations

For the simulations, the physical parameters including slip length, surface tension, contact angle, and material density for $PM_{2.5}$ were needed. Table S2 shows the values used for these physical parameters in the simulations. The lower and upper limits of the slip length used in the simulations were set to 5 nm and 10 μm, based on literature data of the interactions between fluids and solid surfaces (Schnell, 1956; Churaev et al., 1984; Watanabe et al., 1999; Baudry et al., 2001; Cheng and Giordano, 2002; Tretheway and Meinhart, 2002; Jin et al., 2004; Joseph and Tabeling, 2005; Choi and Kim, 2006; Zhu et al., 2012; Li et al., 2014). To capture the full plausible range of $PM_{2.5}$ viscosities

in the poke-and-flow simulations, we selected upper and lower bounds for density and surface tension based on representative aerosol types from prior studies. For the lower bound, we used properties of isoprene-derived SOA, density of 1.2 g cm^{-3} (Li et al., 2022) and surface tension of 17 mN m^{-1} (https://www.chemspider.com/), typical of organic-rich aerosol systems that readily exhibit flow behavior. For the upper bound, we applied values for supersaturated AS, assigning a density of 1.7 g cm^{-3} (https://www.chemspider.com/) and a surface tension of 95 mN m^{-1} (Mikhailov et al., 2024), representing highly concentrated inorganic aerosol solutions. Although the sampled $PM_{2.5}$ is mostly organic, inorganic salts such as AS are common and, under dry or aged conditions, can become highly concentrated and strongly inhibit particle flow. Using supersaturated AS, therefore, provides a conservative high-viscosity limit, ensuring the simulations encompass the full transition from flow to non-flow without implying that the particles themselves are fully inorganic.

Moreover, the measured contact angles for these droplets ranged from 30° to 75°, reflecting the experimentally measured diversity in particle-substrate wetting characteristics. Additional simulation inputs included the inner and outer diameters of the torus geometry, which were determined from optical images acquired after poking the particles. The uncertainty of approximately two orders of magnitude in the viscosity measurement stems from the variability in the key parameters used in the simulation (i.e., slip length, surface tension, density, and contact angle). Among these parameters, the slip length was the primary contributor to the uncertainty in viscosity, as reported in previous investigations (Grayson et al., 2015; Song et al., 2015).

S4. Conditioning time of $PM_{2.5}$ droplets under controlled RH conditions

In the poke-and-flow experiment, $PM_{2.5}$ droplets with a diameter of ~40 μm were deposited on a hydrophobic substrate and allowed to equilibrate under the specified RH of the carrier gas. To verify whether the droplets approached near-equilibrium with the target RH, we applied a previously established method that incorporates measured viscosity values and the corresponding water diffusion coefficient (Evoy et al., 2021; Maclean et al., 2021; Smith et al., 2021; Kiland et al., 2023). This approach compares the experimental conditioning time with the characteristic mixing time of water within organic aerosol (OA), $\tau_{mix,\,H_2O}$, calculated as follows:

$$\tau_{mix,H2O} = \frac{{d_p}^2}{4\pi^2 D_{H2O}(T,RH)} \quad \text{(S4.1)}$$

Here, d_p represents the particle diameter. $D_{H_2O}(T,\ RH)$ is the RH- and temperature-dependent diffusion coefficient of water in OA. The value of $D_{H_2O}\ (T,\ RH)$ was calculated using the fractional Stokes–Einstein equation, which considers the relationship between viscosity and diffusion when the diffusing species are comparable in size to, or smaller than, the molecules forming the matrix (Evoy, 2020):

$$D_{H2O}(T,RH) = D^{\circ}{}_{H2O}(T) \times \left(\frac{\eta^{\circ}{}_{H2O}(T)}{\eta(T,\ RH)}\right)^{\xi} \quad \text{(S4.2)}$$

In this equation, $D^{\circ}{}_{H_2O}(T)$ is the self-diffusion of water calculated with the Stokes-Einstein equation at 290 K (2.12×10^{-9} m^2 s^{-1}). $\eta^{\circ}{}_{H2O}(T)$ is the viscosity of pure water obtained from literature with a value of ~1×10^{-3} Pa·s at 290 K (Weight, 2019). $\eta(T,RH)$ is the measured viscosity of the $PM_{2.5}$ droplet at the corresponding RH and temperature. ξ

is the fractional exponent obtained using Eq. (S4.3), which accounts for the relative size of the diffusing molecule and the surrounding matrix:

$$\xi = 1 - \left[A \times exp\left(-B\frac{r_{diff}}{r_{matrix}}\right)\right] \quad \text{(S4.3)}$$

where coefficient values of A = 0.73 and B = 1.79 (Evoy et al., 2020), the hydrodynamic radius of water was taken as r_{diff} = 0.1 nm (Price et al., 2016), and the hydrodynamic radius of the matrix molecule was fixed at $r_{\text{matrix}} = 0.44$ nm. Using this value in Eq. (S4.3) yields a fractional exponent of ξ = 0.51. The conditioning time used in this study is summarized in Table S1.

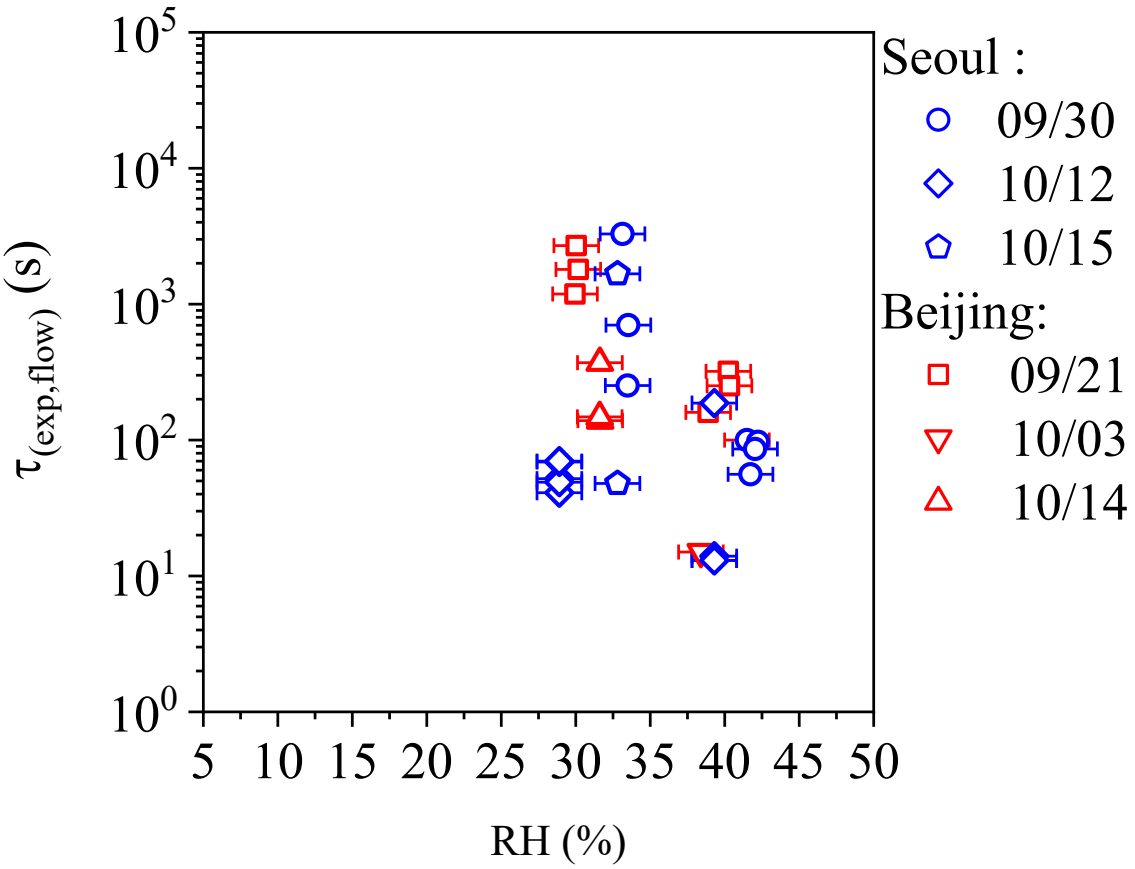

Figure S1. Characteristic experimental flow time ($\tau_{exp,\,flow}$) of $PM_{2.5}$ droplets determined using the poke-and-flow technique for samples collected on different dates in Seoul and Beijing. Each symbol represents an individual $\tau_{exp,\,flow}$ value obtained by poking a single particle at a specific RH. The *x*-axis error bars represent the RH sensor uncertainty (±1.5%), as determined from our RH sensor calibration in the flow cell.

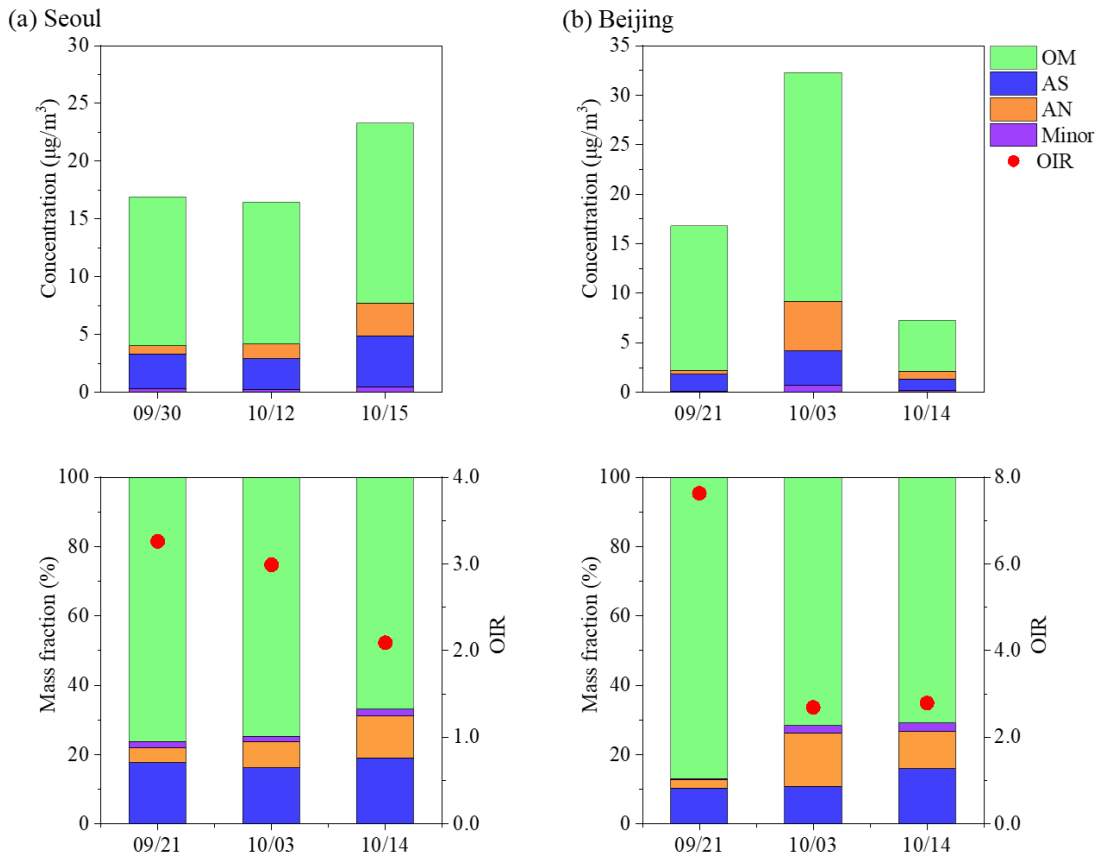

Figure S2. Chemical composition of $PM_{2.5}$ in (a) Seoul and (b) Beijing. For each site, the upper panel shows the concentrations of total $PM_{2.5}$ and its major components, including organic matter (OM), ammonium sulphate (AS), ammonium nitrate (AN), and minor inorganic ions such as Cl^-, Na^+, Ca^{2+}, K^+, and Mg^{2+}. The lower panel shows the corresponding mass fractions (%). The mean OM concentration was estimated by deducing the measured inorganic components from the total $PM_{2.5}$ concentration.

Table S1. Overview of conditioning times for $PM_{2.5}$ droplets under different RH conditions. The parameter τ_{mix,H_2O} represents the characteristic timescale for internal water mixing time within the droplets, derived from the water diffusion coefficient inferred from viscosity at the corresponding RH. The term $\tau_{conditioning}$ refers to the experimentally defined period during which droplets were held at a specified RH to equilibrate with the surrounding gas phase. Calculations were based on a 40 μm droplet diameter, representing the upper-limit droplet size used in the poke-and-flow experiments.

Sample	**RH**	$\tau_{conditioning}$ **(h)**	τ_{mix,H_2O} **(h)**	$\tau_{conditioning} / \tau_{mix,H_2O}$
Seoul (09/30)	41	1.0	0.13	7.6
Seoul (09/30)	33	1.0	0.54	1.9
Seoul (10/12)	39	1.0	0.21	4.7
Seoul (10/12)	29	1.0	0.10	10.5
Seoul (10/12)	33	1.0	0.46	2.2
Beijing (09/21)	40	1.0	0.25	3.9
Beijing (09/21)	30	1.0	0.99	1.0
Beijing (10/03)	38	1.0	0.04	23.0
Beijing (10/14)	32	1.0	0.22	4.6

Table S2. Summary of the key input physical parameters and boundary conditions used in the COMSOL Multiphysics simulations, including the lower and upper bounds of density, surface tension, slip length, and contact angle applied in the modeling. R_0 and r_0 denote the geometric parameters of the torus: R_0 is the distance from the center of the hole to the midpoint of the material ring forming the torus, and r_0 is the radius of that ring.

	Density (g/cm^3)	Surface tension (mN/m)	Slip length[c] (nm)	Contact angle[d] (^{o})
Values for the lower limit	1.2	17	5	30 (if $(R_o - r_o)/r_o < 2$) 75 (if $(R_o - r_o)/r_o > 2$)
Values for upper limit	1.7	95	10000	75 (if $(R_o - r_o)/r_o < 2$) 30 (if $(R_o - r_o)/r_o > 2$)

[c]The range based on slip length measurements on hydrophobic surfaces (Schnell, 1956; Churaev et al., 1984; Watanabe et al., 1999; Baudry et al., 2001; Cheng and Giordano, 2002; Tretheway and Meinhart, 2002; Jin et al., 2004; Joseph and Tabeling, 2005; Choi and Kim, 2006; Zhu et al., 2012; Li et al., 2014). [d]Since the contact angle represents an average value derived from a selection of samples, it is set over a wide range.

References

Baudry, J., Charlaix, E., Tonck, A., and Mazuyer, D.: Experimental evidence for a large slip effect at a nonwetting fluid−solid interface, Langmuir, 17, 5232–5236, https://doi.org/10.1021/la0009994, 2001.

Cheng, J.-T. and Giordano, N.: Fluid flow through nanometer-scale channels, Phys. Rev. E, 65, 031206, https://doi.org/10.1103/PhysRevE.65.031206, 2002.

Choi, C.-H. and Kim, C.-J.: Large slip of aqueous liquid flow over a nanoengineered superhydrophobic surface, Phys. Rev. Lett. , 96, 066001, https://doi.org/10.1103/PhysRevLett.96.066001, 2006.

Choi, J. H., Ryu, J., Jeon, S., Seo, J., Yang, Y.-H., Pack, S. P., Choung, S., and Jang, K.-S.: In-depth compositional analysis of water-soluble and -insoluble organic substances in fine (PM2.5) airborne particles using ultra-high-resolution 15T FT-ICR MS and GC×GC-TOFMS, Environ. Pollut., 225, 329–337, https://doi.org/10.1016/j.envpol.2017.02.058, 2017.

Churaev, N. V., Sobolev, V. D., and Somov, A. N.: Slippage of liquids over lyophobic solid surfaces, J. Colloid Interface Sci., 97, 574–581, https://doi.org/10.1016/0021-9797(84)90330-8, 1984.

Evoy, E.: The relationship between diffusion coefficients and viscosity in organic-water matrices as proxies for secondary organic aerosol, PHD thesis, The University of British Columbia, Vancouver, Canada, 2020.

Evoy, E., Kamal, S., Patey, G. N., Martin, S. T., and Bertram, A. K.: Unified description of diffusion coefficients from small to large molecules in organic–water mixtures, J. Phys. Chem. A, 124, 2301–2308, https://doi.org/10.1021/acs.jpca.9b11271, 2020.

Evoy, E., Kiland, K. J., Huang, Y., Schnitzler, E. G., Maclean, A. M., Kamal, S., Abbatt, J. P. D., and Bertram, A. K.: Diffusion coefficients and mixing times of organic molecules in β-caryophyllene secondary organic aerosol (SOA) and biomass burning organic aerosol (BBOA), ACS Earth Space Chem., 5, 3268–3278, https://doi.org/10.1021/acsearthspacechem.1c00317, 2021.

Grayson, J. W., Song, M., Sellier, M., and Bertram, A. K.: Validation of the poke-flow technique combined with simulations of fluid flow for determining viscosities in samples with small volumes and high viscosities, Atmos. Meas. Tech., 8, 2463–2472, https://doi.org/10.5194/amt-8-2463-2015, 2015.

Jin, S., Huang, P., Park, J., Yoo, J. Y., and Breuer, K. S.: Near-surface velocimetry using evanescent wave illumination, Exp. Fluids, 37, 825–833, https://doi.org/10.1007/s00348-004-0870-7, 2004.

Joseph, P. and Tabeling, P.: Direct measurement of the apparent slip length, Phys. Rev. E., 71, 035303, https://doi.org/10.1103/PhysRevE.71.035303, 2005.

Kiland, K. J., Mahrt, F., Peng, L., Nikkho, S., Zaks, J., Crescenzo, G. V., and Bertram, A. K.: Viscosity, glass formation, and mixing times within secondary organic aerosol from biomass burning phenolics, ACS Earth Space Chem., 7, 1388–1400, https://doi.org/10.1021/acsearthspacechem.3c00039, 2023.

Kim, N. K., Kim, Y. P., Ghim, Y. S., Song, M. J., Kim, C. H., Jang, K. S., Lee, K. Y., Shin, H. J., Jung, J. S., Wu, Z., Matsuki, A., Tang, N., Sadanaga, Y., Kato, S., Natsagdorj, A., Tseren-Ochir, S., Baldorj, B., Song, C.-K., and Lee, J. Y.: Spatial distribution of PM2.5 chemical components during winter at five sites in Northeast Asia: High temporal resolution measurement study, Atmos. Environ., 290, 119359, https://doi.org/10.1016/j.atmosenv.2022.119359, 2022.

Lan, Z., Zhang, B., Huang, X., Zhu, Q., Yuan, J., Zeng, L., Hu, M., and He, L.: Source apportionment of PM2.5 light extinction in an urban atmosphere in China, J. Environ. Sci., 63, 277–284, https://doi.org/10.1016/j.jes.2017.07.016, 2018.

Li, K., Zhang, X., Zhao, B., Bloss, W. J., Lin, C., White, S., Yu, H., Chen, L., Geng, C., Yang, W., Azzi, M., George, C., and Bai, Z.: Suppression of anthropogenic secondary organic aerosol formation by isoprene, npj Clim. Atmos. Sci., 5, 12, https://doi.org/10.1038/s41612-022-00233-x, 2022.

Li, L., Mo, J., and Li, Z.: Flow and slip transition in nanochannels, Phys. Rev. E, 90, 033003–033003, https://doi.org/10.1103/physreve.90.033003, 2014.

Maclean, A. M., Li, Y., Crescenzo, G. V., Smith, N. R., Karydis, V. A., Tsimpidi, A. P., Butenhoff, C. L., Faiola, C., Lelieveld, J., Nizkorodov, S. A., Shiraiwa, M., and Bertram, A. K.: Global distribution of the phase state and mixing times within secondary organic aerosol particles in the troposphere based on room-temperature viscosity measurements, ACS Earth Space Chem., 5, 3458–3473, https://doi.org/10.1021/acsearthspacechem.1c00296, 2021.

Mikhailov, E. F., Vlasenko, S. S., and Kiselev, A. A.: Water activity and surface tension of aqueous ammonium sulfate and D-glucose aerosol nanoparticles, Atmos. Chem. Phys., 24, 2971–2984, https://doi.org/10.5194/acp-24-2971-2024, 2024.

Price, H. C., Mattsson, J., and Murray, B. J.: Sucrose diffusion in aqueous solution, Phys. Chem. Chem. Phys., 18, 19207–19216, https://doi.org/10.1039/c6cp03238a, 2016.

Qiu, Y., Wu, Z., Man, R., Zong, T., Liu, Y., Meng, X., Chen, J., Chen, S., Yang, S., and Yuan, B.: Secondary aerosol formation drives atmospheric particulate matter pollution over megacities (Beijing and Seoul) in East Asia, Atmos. Environ., 301, 119702, https://doi.org/10.1016/j.atmosenv.2023.119702, 2023.

Schnell, E.: Slippage of water over nonwettable surfaces, J. Appl. Phys., 27, 1149–1152, https://doi.org/10.1063/1.1722220, 1956.

Smith, N. R., Crescenzo, G. V., Huang, Y. Z., Hettiyadura, A. P. S., Siemens, K., Li, Y., Faiola, C. L., Laskin, A., Shiraiwa, M., Bertram, A. K., and Nizkorodov, S. A.: Viscosity and liquid-liquid phase separation in healthy and stressed plant SOA, Environ. Sci.: Atmos., 1, 140–153, https://doi.org/10.1039/d0ea00020e, 2021.

Song, M., Liu, P., Hanna, S. J., Li, Y. J., Martin, S. T., and Bertram, A. K.: Relative humidity-dependent viscosities of isoprene-derived secondary organic material and atmospheric implications for isoprene-dominant forests, Atmos. Chem. Phys., 15, 5145–5159, https://doi.org/10.5194/acp-15-5145-2015, 2015.

Song, M., Jeong, R., Kim, D., Qiu, Y., Meng, X., Wu, Z., and Ahn, J.: Comparison of phase states of PM2.5 over megacities, Seoul and Beijing, and their implications on particle size distribution, Environ. Sci. Technol., 56, 17581–17590, https://doi.org/10.1021/acs.est.2c06377, 2022.

Song, M., Li, Y., Seong, C., Yang, H., Jang, K.-S., Wu, Z., Lee, J. Y., Matsuki, A., and Ahn, J.: Direct observation of liquid–liquid phase separation and core–shell morphology of PM2.5 collected from three Northeast Asian cities and implications for N2O5 hydrolysis, ACS ES&T Air, 2, 1079–1088, https://doi.org/10.1021/acsestair.5c00043, 2025.

Tretheway, D. C. and Meinhart, C. D.: Apparent fluid slip at hydrophobic microchannel walls, Phys. Fluids, 14, L9–L12, https://doi.org/10.1063/1.1432696, 2002.

Watanabe, K., Udagawa, Y., and Udagawa, H.: Drag reduction of Newtonian fluid in a circular pipe with a highly water-repellent wall, J. Fluid Mech., 381, 225–238, https://doi.org/10.1017/S0022112098003747, 1999.

Weight, W. D.: Practical Hydrogeology: Principles and field applications, McGraw Hill Professional, Newyork, 2019.

Won, S. R., Lee, K., Song, M., Kim, C., Jang, K.-S., and Lee, J. Y.: Characteristic of PM2.5 concentration and source apportionment during winter in Seosan, Korea, Asian J. Atmos. Environ., 18, 22, https://doi.org/10.1007/s44273-024-00044-x, 2024.

Xue, Q., Liu, X., Tian, Y., and Feng, Y.: Variations of inhalation risks during different heavy pollution episodes based on 3-year measurement of toxic components in size-segregated particles, Sci. Total Environ., 880, 163234, https://doi.org/10.1016/j.scitotenv.2023.163234, 2023.

Zhu, L., Neto, C., and Attard, P.: Reliable measurements of interfacial slip by colloid probe atomic force microscopy. III. Shear-rate-dependent slip, Langmuir, 28, 3465–3473, 2012.